STATISTICS, OPTIMIZATION AND INFORMATION COMPUTING
Stat., Optim. Inf. Comput., Vol. **14**, July 2025, pp 0–24.
Published online in International Academic Press (www.IAPress.org)

Power Flow Analysis in Unbalanced Distribution Networks with Single-Phase and Two-Phase Laterals Using a Fixed-Point Formulation Implemented in MATLAB

Cristian David Cuervo-González, John Fredy Pinilla-Morales, Oscar Danilo Montoya

Facultad de Ingeniería, Universidad Distrital Francisco José de Caldas, Bogotá D.C. 110121, Colombia

Abstract This paper proposes a fixed-point methodology for power flow analysis in unbalanced three-phase distribution networks featuring mixed single-phase, two-phase, and three-phase laterals—a common configuration in rural and low-voltage distribution systems. The method addresses the convergence challenges posed by low *X/R* ratios, radial topologies, and inherent phase unbalance that hinder classical power flow solvers. The formulation employs a per-unit impedance model, constructs a detailed three-phase nodal admittance matrix, and incorporates explicit mathematical models for wye and delta load connections. A fixed-point iterative scheme updates nodal voltages using a partitioned network representation. The algorithm was implemented in MATLAB® and validated against the industry-standard software DIgSILENT PowerFactory® using three test systems of 4, 8, 25 and 124 nodes. Results demonstrate exceptional accuracy, with voltage magnitude deviations below 2×10^{-3} p.u., phase angle differences under $0.05°$, and relative power balance errors consistently below 0.05%. The method exhibits robust and rapid convergence, reaching a tolerance of $\varepsilon = 1 \times 10^{-10}$ in only 4 iterations across all test cases, with near-linear computational scalability. This was observed with standard load systems, but to test the methodology's performance with heavy load systems, the active power consumed by the loads was increased tenfold. We observed that execution times and the number of iterations increased, and also that, as the system load increased, the method became less contractive. This combination of high numerical precision, deterministic convergence, and low computational cost establishes the proposed fixed-point method as an effective and reliable tool for the analysis and planning of modern, unbalanced distribution networks.

Keywords Distribution system analysis; Unbalanced power flow; Fixed-point method; Mixed-phase laterals; Three-phase admittance matrix; Load modeling (wye/delta)

DOI: 10.19139/soic-2310-5070-3443

1. Introduction

The reliable, resilient, and efficient supply of electrical energy is a cornerstone of technological, industrial, and societal advancement, as evidenced by the well-established correlation between electricity consumption and key economic indicators such as gross domestic product, capital formation, and labor productivity [1]. Consequently, electric power systems (EPS) demand meticulous design, operation, and maintenance under rigorous quality standards, supported by robust infrastructure to ensure secure and economical energy delivery from generation sources to end-users [2]. Within this framework, distribution networks are of paramount importance. As the most extensive and consumer-proximate component of the EPS, they constitute a critical interface and a nexus of significant operational complexity [3].

Historically, distribution networks in many Latin American contexts have received less planning and investment priority compared to generation and transmission systems [4]. This under-prioritization has contributed to elevated

*Correspondence to: O. D. Montoya (Email: odmontoyag@udistrital.edu.co). Facultad de Ingeniería, Universidad Distrital Francisco José de Caldas, Bogotá D.C. 110121, Colombia.

ISSN 2310-5070 (online) ISSN 2311-004X (print)

levels of technical and non-technical losses, undermining both the efficiency and quality of electricity supply [5]. Currently, technical losses—which are physically governed by current magnitudes and circuit resistances as described by Joule's law—account for approximately 70% of total losses in distribution systems (DS) [6,7].

Addressing these challenges requires robust analytical tools for modeling and assessing network performance. Power flow analysis has emerged as an indispensable methodology in this context, enabling the determination of system operating states, the evaluation of voltage profiles, and the identification of potential overloads and losses across network segments [8]. As such, it forms the essential computational foundation for the efficient planning, operation, and strategic expansion of EPS, with direct applicability to DS [9,10].

The evolution of power flow methodologies reflects the growing complexity of power systems. Early approaches relied on simplified, often manual calculations suited only to small-scale or highly aggregated systems [11]. The advent of computational technology enabled a paradigm shift, leading to robust numerical algorithms such as Gauss-Seidel and Newton-Raphson, which facilitated the analysis of larger, more complex, and meshed transmission networks [12]. However, these classical techniques often encounter significant convergence difficulties when applied to modern distribution systems. These challenges stem from distinct topological and electrical characteristics, including a low X/R ratio, inherent phase unbalance, and radial or weakly meshed structures—features that are prevalent in networks with extensive single-phase and two-phase laterals [13].

In response to these limitations, specialized algorithms tailored for distribution systems have been developed. One widely used approach is the backward/forward sweep method, which systematically applies Kirchhoff's laws in radial networks—a typical distribution system configuration [14]. Its performance has been enhanced through acceleration techniques such as the Anderson Mixing Scheme, which improves convergence in systems with a low X/R ratio [15].

Another promising approach is the successive approximations (or fixed-point) method, recognized for its computational efficiency and adaptability to diverse distribution network topologies [16, 17]. In terms of convergence, it presents advantages over the NR method by offering a more robust performance in distribution systems with low X/R ratios, where the inversion of the Jacobian matrix usually presents numerical problems [18]. Likewise, with respect to the BFS method, it presents advantages in terms of convergence since the fixed-point method does not have topological restrictions in radial networks that may compromise convergence [19].

Progress in scientific computing and high-level programming environments has further accelerated the development of these methods. Platforms such as MATLAB, Julia, and Python enable the implementation, testing, and validation of sophisticated algorithms on networks of realistic scale and complexity [20–22]. In particular, MATLAB provides a flexible framework for algorithmic development, facilitating straightforward validation against industry-standard tools like DIgSILENT PowerFactory, which is widely employed for technical studies of real-world operational scenarios [23]. However, this type of commercial tools typically operates as black-box systems, which limits the ability to internally modify models and algorithms, thereby restricting their flexibility to directly address more specific or emerging research problems.

Despite these developments, a significant research gap persists in the power flow analysis of distribution systems with unbalanced single-phase and two-phase laterals—a common configuration in rural networks [24] that remains underexplored in the technical literature. Such mixed topologies exacerbate the convergence challenges of classical methods and necessitate more refined mathematical models to accurately represent the heterogeneity of modern distribution networks. Moreover, there is a clear need for methodologies that are both scalable and easily validatable to bridge the gap between academic research and practical industrial application [25].

Motivated by this need, this article proposes a computational methodology that is not novel in terms of introducing a new method, but rather in integrating fundamental features for power flow analysis in unbalanced distribution networks with single-phase, two-phase, and three-phase laterals, including both delta and wye configurations. These features include the incorporation of topologies that are not necessarily meshed, the representation of mutual impedances, robust convergence performance in networks with low X/R ratios, and the use of open-source software which, by its nature, can be further extended to incorporate additional aspects of power systems, such as optimization studies, the integration of distributed energy resources (DER), and the impact of remotely controlled equipment.

The approach is based on the fixed-point method and is implemented in the MATLAB environment. The main objective is to provide an effective tool for the study of complex network topologies that pose significant challenges to conventional solution methods. The proposed methodology will be validated through a comparative analysis with results obtained from the industry-standard software DIgSILENT PowerFactory. This validation will employ test networks of 4, 8, 25 and 124 nodes to rigorously assess the accuracy of the algorithm, its convergence behavior, its practical applicability, and its scalability against a widely adopted industry benchmark [26].

The remainder of this paper is organized as follows. Section 3 presents the mathematical formulation of the fixed-point-based power flow model. Section 4 details the computational implementation of the proposed methodology in MATLAB. Section 6 describes the validation scenarios and presents a comparative analysis of the results. Finally, Section 7 provides concluding remarks and outlines directions for future work.

2. Related Work

2.1. Classical Methods in Unbalanced Networks

Power flow analysis for electrical networks has been extensively studied in recent years. Among the classical methods are Newton-Raphson, Gauss-Seidel, and Fast Decoupled Load Flow, which have been predominantly used in transmission systems. In radial distribution systems, the backward/forward sweep method is commonly applied.

The Newton-Raphson method is one of the most widely used due to its quadratic convergence properties and high numerical accuracy. This method is based on the linearization of the power flow equations through the use of the Jacobian matrix; however, its performance decreases in distribution systems with low X/R ratios [27].

The Gauss-Seidel method follows an iterative approach that updates nodal voltages sequentially. This method is simple to implement; however, it exhibits slow convergence, making it unsuitable for large-scale or highly complex systems [28].

The Fast Decoupled Load Flow method is an alternative to Newton-Raphson that exploits the weak coupling between active and reactive power. This method significantly reduces computational effort, but since it is based on Newton-Raphson, it shares similar limitations when applied to distribution systems with low X/R ratios [28].

The backward/forward sweep method is commonly used to solve power flow problems in distribution networks due to its simplicity and efficiency in radial topologies. This method is based on sequential backward and forward traversals of the network to compute currents and voltages. However, its application to meshed systems presents challenges and requires network radialization or loop compensation techniques [29].

2.2. Fixed-Point and Successive Approximation Methods

In recent years (2023–2025), power flow for distribution systems has been studied with approaches that are oriented toward providing greater computational efficiency and robustness. Under the previous context, fixed-point methods have been enhanced through techniques that accelerate convergence; one of them is the Anderson acceleration method, which, through data from previous iterations, constructs better approximations to the solution [30].

Anderson acceleration is a complement to the classical fixed-point method, which has a convergence factor that, compared to the classical one, is significantly reduced by combining previous iterations through a least-squares problem, while the classical method normally presents linear convergence. Recent studies [31] have demonstrated that this complement, in addition to improving the number of iterations, improves the convergence rate, making it an interesting tool for engineering applications.

However, this numerical improvement requires greater computational deployment for each iteration, since it stores information from previous iterations, in addition to solving auxiliary systems in each iteration [32]. In contrast, the classical method presents greater computational ease, making it simpler and more predictable, which is advantageous for implementation in large-scale systems [33].

In parallel, other complements have emerged, but with different foundations; among them, the use of graph theory [34], machine learning [35], and neural networks [36] stands out, whose objective is to accelerate the solution of complex and large-scale systems, but with high computational requirements.

Given the above, despite the implementation of new techniques that are mathematically superior, it is necessary to find a balance with computational complexity when deploying the tool. This work is precisely oriented toward seeking mathematical rigor without sacrificing computational simplicity.

2.3. Open-Source Implementations (MATLAB, Julia, Python)

The emergence of high-level open-source programming languages has facilitated the implementation of power flow algorithms and the validation of new methodologies. Among these programming environments, MATLAB (MATPOWER), Julia, and Python stand out, where, as time progresses, new specialized libraries are continuously being developed. Among these, the following can be highlighted:

In the Python ecosystem, Pandapower is an open-source library widely used in research and academia that supports power flow analysis in distribution networks and includes Optimal Power Flow (OPF) capabilities. This tool can solve power flow problems using multiple methods, such as the classical Newton-Raphson and Gauss-Seidel approaches, as well as more specialized methods like the backward/forward sweep (BFS), which is mainly applied to radial networks [37].

PYPOWER is a Python-based version of MATPOWER. This tool can solve power flow problems using Newton-Raphson and OPF formulations.

In Julia, PowerModelsDistribution.jl was developed for the analysis and optimization of electrical distribution networks. This library formulates the power flow problem as an optimization problem [33].

In MATLAB, MATPOWER is a widely used tool that solves power flow problems using Newton-Raphson, Gauss-Seidel, and OPF formulations. However, it does not handle unbalanced three-phase networks or mixed-phase laterals up to version 8, which is still considered a prototype and addresses these features through a mathematical model solved using nonlinear optimization techniques [38].

2.4. Research Gap Addressed in This Work

Through the review conducted in the previous subsections, important limitations in the power flow analysis problem are identified, particularly in distribution systems. Existing methodologies, along with their various extensions, tend to partially address the characteristics of real networks, especially in the presence of unbalances, mixed-phase laterals, and different topological configurations.

Classical methods such as the backward/forward sweep (BFS) present restrictions, mainly in meshed topologies [39], which limits their direct application to this type of networks. Additionally, the nature of the method does not allow for a general mathematical formulation, making it difficult to evaluate convergence.

On the other hand, the fixed-point method provides an explicit representation of the power flow problem, in which the nodal voltages are expressed as a nonlinear transformation of themselves, that is, $V = f(V)$. This representation allows solving in a direct and natural way both radial and meshed topologies by making use of the nodal admittance matrix, without requiring structural modifications to the algorithm [40].

In contrast, the backward/forward sweep (BFS) method is inherently algorithmic and is mainly designed for radial systems, since it is based on backward and forward traversals along the feeder structure. Although modifications of BFS have been proposed for meshed topologies, these approaches usually require network radialization techniques or loop compensation, which increases algorithmic complexity and reduces generality.

This distinction is fundamental from a theoretical point of view. The mathematical structure of the fixed-point formulation allows the application of well-established analytical tools, such as the contraction mapping theorem, spectral radius analysis, and convergence evaluation through the Jacobian. As a result, it is possible to formally establish sufficient conditions for the convergence of the method. In contrast, the backward/forward sweep approach does not admit a compact functional representation of the form $V = f(V)$, which limits the possibility of performing a rigorous convergence analysis and, in many cases, leads to a more empirical validation of its performance.

In recent years, formulations based on the Banach fixed-point theorem have been proposed for power flow analysis in distribution systems. These methodologies reformulate the problem as a fixed-point equation in terms of nodal voltages or currents, allowing the use of successive approximation schemes. Among their main advantages are the possibility of establishing formal convergence conditions, greater numerical stability, and a more general formulation that does not depend on a radial network topology. These characteristics are especially relevant in the analysis of unbalanced systems with mixed-phase laterals.

In this context, this paper presents a tool based on the fixed-point method, implemented in MATLAB, which integrates capabilities that are commonly found separately. It combines unbalanced distribution networks with mixed-phase laterals and mixed load configurations, while being applicable to both radial and meshed networks without requiring fundamental modifications to the algorithm. Additionally, it maintains a low computational burden with strong convergence performance, even under low X/R ratio conditions.

3. Mathematical formulation

This section details the mathematical framework of the proposed fixed-point power flow method for unbalanced distribution networks with mixed-phase laterals. The formulation begins by establishing the per-unit system and modeling the network topology using incidence matrices. Subsequently, it presents the derivation of the three-phase nodal admittance matrix, the handling of diverse load configurations, and the iterative fixed-point voltage update equation. The complete set of equations for calculating line currents, technical losses, and generated power is also provided, constituting the core analytical foundation for the computational implementation discussed in the following section.

3.1. System bases

The following base quantities are defined for the per-unit (p.u.) representation of the system:

$$Z_b = \frac{V_b^2}{S_b}, \tag{1}$$

$$I_b = \frac{S_b}{\sqrt{3} \cdot V_b}, \tag{2}$$

where V_b denotes the base voltage, S_b the base power, Z_b the base impedance, and I_b the base current.

3.2. Network topology and modeling

The network topology is described using an incidence matrix $\mathbf{A} \in \mathbb{R}^{N \times L}$, where N denotes the number of nodes and L the number of branches. Each element A_{ij} indicates the connection relationship between node i and branch j. The per-unit impedance of each branch l is given by:

$$z_l = \frac{R_l + jX_l}{Z_b}, \tag{3}$$

where R_l and X_l are the respective resistance and reactance of branch l, and Z_b is the base impedance defined in Section 3.1.

3.3. Three-phase nodal admittance

The network is represented in a three-phase framework using expanded nodal quantities. The three-phase bus admittance matrix is constructed as:

$$\mathbf{Y}_{\text{bus}}^{3\phi} = \mathbf{A}_{3\phi}\, \mathbf{Z}_{3\phi}^{-1}\, \mathbf{A}_{3\phi}^{\top}, \tag{4}$$

where $\mathbf{A}_{3\phi} \in \mathbb{R}^{3N \times 3L}$ is the three-phase incidence matrix, $\mathbf{Z}_{3\phi}$ is a diagonal matrix containing the per-phase branch impedances in per-unit, and $(\cdot)^{\top}$ denotes the matrix transpose.

This formulation captures the mutual coupling between phases and provides a complete representation for unbalanced power flow analysis.

3.4. Block separation of the admittance matrix

To facilitate the power flow solution, the three-phase admittance matrix is partitioned with respect to the slack (reference) node. Let the set of all nodes be divided into:

- The slack node (subscript s),
- The remaining demand (non-slack) nodes (subscript d).

The admittance matrix is accordingly partitioned into the following submatrices:

$$\mathbf{Y}_{dd}^{3\phi} : \text{Admittance block between demand nodes,} \tag{5}$$

$$\mathbf{Y}_{ds}^{3\phi} : \text{Admittance block coupling demand nodes to the slack node.} \tag{6}$$

This block structure is used to isolate the unknown demand node voltages in the subsequent fixed-point iteration.

3.5. Slack node voltage

The slack bus (node 1) is modeled as an ideal balanced three-phase voltage source. Its per-unit voltage phasors are defined as:

$$\mathbf{V}_s = V_{\text{slack}} \begin{bmatrix} 1 \\ e^{-j2\pi/3} \\ e^{j2\pi/3} \end{bmatrix}, \tag{7}$$

where V_{slack} is the specified line-to-neutral voltage magnitude at the slack bus. This balanced, positive-sequence representation provides the reference angle and voltage magnitude for the entire network.

3.6. Load Model and Complex Power

The electrical load at a network bus k is modeled as a three-phase complex power vector, representing the net injected power (generation minus consumption) into the node. It is defined as

$$\mathbf{S}_k \triangleq \mathbf{P}_k + j\mathbf{Q}_k \in \mathbb{C}^{3\times 1}, \tag{8}$$

where $\mathbf{P}_k = [P_k^a, P_k^b, P_k^c]^T \in \mathbb{R}^{3\times 1}$ and $\mathbf{Q}_k = [Q_k^a, Q_k^b, Q_k^c]^T \in \mathbb{R}^{3\times 1}$ are the vectors of active and reactive power for phases a, b, and c, respectively. The complex power $\mathbf{S}_k$ constitutes the primary load specification for subsequent power flow analysis and forms the essential link between network voltages, currents, and power consumption.

3.7. Calculation of nodal currents

The nodal current injection vector $\mathbf{I}_k$ at bus k is derived from the complex power load $\mathbf{S}_k$ and the nodal phase-to-neutral voltage vector $\mathbf{V}_k$ via the power balance equation $\mathbf{S}_k = \operatorname{diag}(\mathbf{V}_k)\,\mathbf{I}_k^*$. The specific formulation depends on the load-connection topology.

3.7.1. Star (Wye) Connection For a three-phase load connected in a star (wye) configuration, the line currents are identical to the phase currents. The current injection follows directly from the power balance:

$$\mathbf{I}_k^{\mathrm{Y}} = \text{diag}\left(\mathbf{V}_k^*\right)^{-1} \mathbf{S}_k^*. \tag{9}$$

3.7.2. Delta (Δ) Connection For a delta-connected load the complex power is defined across the phase-to-phase voltages. Introducing the transformation matrices

$$\mathbf{M} \triangleq \begin{bmatrix} 1 & -1 & 0 \\ 0 & 1 & -1 \\ -1 & 0 & 1 \end{bmatrix}, \qquad \mathbf{H} \triangleq \begin{bmatrix} 0 & 0 & 1 \\ 1 & 0 & 0 \\ 0 & 1 & 0 \end{bmatrix}, \tag{10}$$

where $\mathbf{M}$ yields the forward phase-to-phase voltage vector $\mathbf{V}_k^{\mathrm{ab,bc,ca}} = \mathbf{M}\,\mathbf{V}_k$, the nodal current injection is obtained as the sum of contributions from the forward and reverse branch paths:

$$\mathbf{I}_k^{\Delta} = \operatorname{diag}\left(\mathbf{M}\,\mathbf{V}_k^{*}\right)^{-1}\mathbf{S}_k^{*} + \operatorname{diag}\left(\mathbf{M}^T\mathbf{V}_k^{*}\right)^{-1}\mathbf{H}\,\mathbf{S}_k^{*}. \tag{11}$$

The first term corresponds to currents injected from the forward phase-to-phase paths; the second term accounts for the reverse paths, with the permutation matrix $\mathbf{H}$ aligning the power vector with the appropriate voltage. This formulation guarantees a consistent power balance for a delta-connected load when observed at the network nodes.

3.8. *Voltage update via fixed-point iteration*

The three-phase voltages at the demand (load) buses are solved iteratively using a fixed-point method derived from the network impedance model. The voltage vector for all demand buses, $\mathbf{V}_d \in \mathbb{C}^{3n_d\times 1}$, is updated at iteration $t+1$ according to

$$\mathbf{V}_d^{t+1} = -\mathbf{Z}_{dd}^{3\phi}\left(\mathbf{I}_d^{t} + \mathbf{Y}_{ds}^{3\phi}\,\mathbf{V}_s\right), \tag{12}$$

where $\mathbf{Z}_{dd}^{3\phi} \in \mathbb{C}^{3n_d\times 3n_d}$ is the three-phase impedance matrix for the demand sub-network, $\mathbf{Y}_{ds}^{3\phi} \in \mathbb{C}^{3n_d\times 3n_s}$ is the mutual admittance matrix linking demand and source buses, $\mathbf{V}_s \in \mathbb{C}^{3n_s\times 1}$ is the vector of fixed source-bus (substation) voltages, and $\mathbf{I}_d^{t}$ is the vector of current injections at the demand buses computed from the voltages at iteration t via the load models of Section 3.7.

The iteration is terminated when the maximum change in voltage magnitude across all phases and all demand buses between consecutive iterations falls below a specified tolerance $\varepsilon > 0$:

$$\max_{k\in\mathcal{D},\,\phi\in\{a,b,c\}}\left\{\left|\,|V_{d,k,\phi}^{t+1}| - |V_{d,k,\phi}^{t}|\,\right|\right\} < \varepsilon, \tag{13}$$

where $\mathcal{D}$ denotes the set of demand buses. This criterion ensures that the solution has converged to a steady state with respect to voltage magnitudes, which is the primary quantity of interest for power-flow analysis.

3.9. *Line current calculation*

After obtaining the nodal voltage solution $\mathbf{V}_k$ for all buses $k \in \mathcal{N}$, the three-phase current flow in each branch l connecting nodes m and n is calculated using the series impedance of the line. The current vector for branch l is given by

$$\mathbf{I}_l = \mathbf{I}_{mn} = \mathbf{Y}_l^{3\phi}\left(\mathbf{V}_m - \mathbf{V}_n\right), \tag{14}$$

where $\mathbf{Y}_l^{3\phi} = (\mathbf{Z}_l^{3\phi})^{-1} \in \mathbb{C}^{3\times 3}$ is the three-phase series admittance matrix of the branch. For a simple case with decoupled phases and no mutual couplings, this reduces to $\mathbf{Y}_l^{3\phi} = \operatorname{diag}(1/Z_l^{aa}, 1/Z_l^{bb}, 1/Z_l^{cc})$.

3.10. *Calculation of technical losses*

The total active and reactive power losses in the network are computed by summing the contributions from all branches $l = 1,\ldots,L$. For each phase $\phi \in \{a,b,c\}$, the losses are calculated as

$$P_{\text{loss}}^{\phi} = \sum_{l=1}^{L} R_l^{\phi\phi}\left|I_l^{\phi}\right|^2, \tag{15}$$

$$Q_{\text{loss}}^{\phi} = \sum_{l=1}^{L} X_l^{\phi\phi}\left|I_l^{\phi}\right|^2, \tag{16}$$

where $R_l^{\phi\phi} = \Re(Z_l^{\phi\phi})$ and $X_l^{\phi\phi} = \Im(Z_l^{\phi\phi})$ are the series resistance and reactance for phase ϕ of branch l, respectively, and I_l^{ϕ} is the corresponding phase current from (14). The total three-phase loss vectors are $\mathbf{P}_{\text{loss}} = [P_{\text{loss}}^a, P_{\text{loss}}^b, P_{\text{loss}}^c]^T$ and $\mathbf{Q}_{\text{loss}} = [Q_{\text{loss}}^a, Q_{\text{loss}}^b, Q_{\text{loss}}^c]^T$.

3.11. System generation and power balance

The total complex power that must be supplied by the source (substation) to meet the load demand and compensate for losses is determined by enforcing power balance. The generated power per phase is

$$S_{\text{gen}}^{\phi} = \left(P_{\text{load}}^{\phi} + P_{\text{loss}}^{\phi}\right) + j\left(Q_{\text{load}}^{\phi} + Q_{\text{loss}}^{\phi}\right), \quad \phi \in \{a, b, c\}, \tag{17}$$

where $P_{\text{load}}^{\phi} = \sum_{k\in\mathcal{D}} P_k^{\phi}$ and $Q_{\text{load}}^{\phi} = \sum_{k\in\mathcal{D}} Q_k^{\phi}$ are the total active and reactive load demands on phase ϕ, summed over all demand buses $\mathcal{D}$. The total three-phase complex power generated by the system is then

$$S_{\text{gen}}^{\text{total}} = \sum_{\phi\in\{a,b,c\}} S_{\text{gen}}^{\phi} = \mathbf{1}^T \left(\mathbf{S}_{\text{load}} + \mathbf{S}_{\text{loss}}\right), \tag{18}$$

where $\mathbf{S}_{\text{load}} = \sum_{k\in\mathcal{D}} \mathbf{S}_k$ and $\mathbf{S}_{\text{loss}} = \mathbf{P}_{\text{loss}} + j\mathbf{Q}_{\text{loss}}$ are the three-phase vectors of total load and total losses, respectively. This result verifies the conservation of complex power within the network.

3.12. Convergence Conditions of the Fixed-Point Formulation

The convergence analysis of the proposed power flow formulation can be established from the fixed-point theorem. Considering the iterative expression obtained for the network model, the proposed mapping can be written as

$$V_{t+1}^{d} = A + B \cdot \left(\frac{1}{(V_t^d)^*}\right), \tag{19}$$

where A and B are matrices associated with the network parameters and load representation. In particular, these matrices are defined as

$$A = C - Z_{dd}^{Y} Y_{ds} V_s, \tag{20}$$

$$B = -Z_{dd}^{d} \cdot \text{diag}\left((S^d)^*\right). \tag{21}$$

Based on the Banach fixed-point theorem, local convergence toward a fixed point V^* is guaranteed if the spectral radius of the Jacobian matrix associated with the iterative mapping satisfies

$$\rho\left(J(V^*)\right) < 1, \tag{22}$$

where $\rho(\cdot)$ denotes the spectral radius and J corresponds to the Jacobian matrix of the fixed-point mapping.
For the proposed formulation, the Jacobian matrix can be expressed as

$$J = -B \cdot \text{diag}\left(\frac{1}{(V^*)^2}\right). \tag{23}$$

Substituting (23) into the general convergence criterion of (22), the explicit convergence condition of the proposed iterative method is obtained as

$$\rho\left(B \cdot \text{diag}\left(\frac{1}{(V^*)^2}\right)\right) < 1. \tag{24}$$

Since the direct computation of the spectral radius may be computationally expensive for large-scale systems, a sufficient practical condition can be established through any consistent matrix norm, leading to

$$\left\| B \cdot \text{diag}\left(\frac{1}{(V^*)^2}\right) \right\| < 1. \tag{25}$$

Additionally, considering an approximation based on voltage magnitudes, an intuitive convergence criterion can be written as

$$\frac{\|B\|}{|V|^2} < 1. \tag{26}$$

Equation (26) provides a qualitative interpretation of the convergence behavior of the proposed formulation. In this sense, convergence is favored in operating conditions where voltage magnitudes remain sufficiently high and the norm associated with matrix B remains bounded. Consequently, the method exhibits strong convergence properties for practical distribution systems operating under typical loading conditions.

4. Proposed methodology

This work proposes a power flow methodology specifically designed for unbalanced three-phase distribution networks with mixed-phase configurations, including single-phase, two-phase, and three-phase laterals. The core of the algorithm is a fixed-point iteration scheme formulated to solve the nonlinear system of equations governing the network's electrical behavior.

1. **System normalization and per-unit conversion** All system parameters are converted to a common per-unit (p.u.) base. This normalization facilitates a homogeneous treatment of diverse network topologies, reduces numerical sensitivity, and decouples the analysis from specific physical units. Base values for power, voltage, and impedance are defined accordingly.
2. **Topological and electrical network modeling:** The network structure is encoded into mathematical models. A branch matrix is constructed to input the three-phase series impedance parameters for all lines, accounting for self and mutual couplings. A nodal matrix is built to define for each bus its voltage, complex power demand, phase configuration (e.g., A, B, C, AB, BC, CA, ABC), and, for three-phase loads, its connection type (wye or delta). From these, the three-phase incidence matrix $\mathbf{A}$ and the block-diagonal three-phase admittance matrix $\mathbf{Y}_{\text{bus}}^{3\phi}$ are assembled.
3. **Initialization:** The slack (source) bus voltages are initialized as a balanced three-phase positive-sequence set according to:
$$\mathbf{V}_s = V_{\text{base}}\angle[0^\circ,\, -120^\circ,\, 120^\circ]^\top.$$
Voltages at all demand (PQ) buses are initialized, typically as $1.0\angle 0^\circ$ p.u. per phase present. The three-phase power injection vector $\mathbf{S}_d$ is formed from the load data. Convergence tolerance ε and a maximum iteration count $k_{\max}$ are defined.
4. **Calculation of nodal current injections:** The three-phase current injection vector $\mathbf{I}_d^t$ at iteration t is computed from the load power $\mathbf{S}_d$ and the current voltage estimate $\mathbf{V}_d^t$, respecting the specific load connection topology at each node:
$$\mathbf{I}_d^t = \mathcal{F}\left(\mathbf{S}_d, \mathbf{V}_d^t\right),$$
where the function $\mathcal{F}(\cdot)$ implements the wye (Eq. (9)) and delta (Eq. (11)) load models derived in Section 3.7.
5. **Voltage update and convergence check:** Voltages at demand buses are updated using the fixed-point iteration derived from the network impedance model:
$$\mathbf{V}_d^{t+1} = -\mathbf{Z}_{dd}^{3\phi}\left(\mathbf{I}_d^t + \mathbf{Y}_{ds}^{3\phi}\mathbf{V}_s\right).$$
Convergence is assessed by checking if the maximum change in voltage magnitude across all phases and all demand buses between consecutive iterations is below the tolerance:
$$\max\left|\,|\mathbf{V}_d^{(k+1)}| - |\mathbf{V}_d^{(k)}|\,\right| < \varepsilon.$$
If the criterion is not met and $k < k_{\max}$, set $k \leftarrow k+1$ and return to Step 4.

6. **Post-convergence electrical analysis:** Upon convergence, branch currents $\mathbf{I}_l$ are computed via Eq. (14). Total active and reactive power losses per phase, P^{ϕ}_{loss} and Q^{ϕ}_{loss}, are calculated by summing the I^2R and I^2X losses across all branches (Eqs. (15) and (16)). The total complex power required from the slack bus is then determined by the power balance: $\mathbf{S}_{\text{gen}} = \mathbf{S}_{\text{load}} + \mathbf{S}_{\text{loss}}$.
7. **Validation:** The accuracy and robustness of the proposed algorithm are validated by comparing its results against those obtained from established commercial simulation software (DIgSILENT PowerFactory) on standardized test networks (e.g., 4-bus, 8-bus, 25-bus and 125-bus systems).

5. Algorithmic Complexity

The algorithmic complexity of the proposed fixed-point-based methodology can be analyzed using Big-O notation, which describes the growth in the number of operations required for an algorithm to solve a problem as a function of the input system size.

The proposed methodology consists of two main computational stages: a preprocessing stage and an iterative solution stage.

The first computational stage comprises the construction of the three-phase nodal admittance matrix and other matrices associated with the proposed formulation, including matrix inversions, whose algorithmic complexity can be approximated as

$$O(L^3 + N^3) \tag{27}$$

where N corresponds to the number of system nodes and L represents the number of system branches.

Subsequently, the second stage involves an algorithmic complexity associated with matrix-vector multiplications, which can be described as

$$O(N^2) \tag{28}$$

Considering a total of k iterations required to achieve convergence, the overall computational complexity of the proposed methodology can be expressed as

$$O(L^3 + N^3 + kN^2) \tag{29}$$

The previous expression shows that the highest computational cost is concentrated in the first stage, where matrix inversions are performed. However, this stage presents the advantage of being executed only once during the entire solution process of the algorithm.

On the other hand, the iterative process exhibits a quadratic growth with respect to the number of system nodes, which is computationally favorable compared to methods that require repeated matrix factorizations at each iteration. Nevertheless, a potential disadvantage of the proposed approach appears in large-scale systems, where the N^3 term associated with preprocessing may significantly increase computation times and memory usage.

Additionally, the total complexity depends on the number of iterations k required to achieve convergence. Under severe operating conditions, high loading levels, or low X/R ratios, the number of iterations may increase, directly affecting the computational performance of the method. Nevertheless, under normal operating conditions, the proposed formulation presents suitable convergence properties and competitive computational performance for the analysis of medium- and large-scale unbalanced distribution networks.

6. Numerical experiments

To validate the performance and accuracy of the proposed power flow method, comprehensive numerical tests were conducted on three standard unbalanced distribution networks: the 4-bus, 8-bus, 25-bus and 124-bus systems. These test cases represent a range of scales and complexities, including radial topologies, mixed single-phase and three-phase loads, and unbalanced operating conditions. Each system is modeled with detailed per-phase impedance and load data, enabling a thorough evaluation of the algorithm's convergence behavior, computational efficiency, and solution accuracy. The results obtained with the proposed method are compared against those from the commercial software DIgSILENT PowerFactory, which serves as the benchmark for validation.

6.1. The 4-bus test system

The 4-bus system is a small-scale unbalanced radial distribution network comprising 4 nodes, 3 distribution lines, 3 load buses, and one slack bus representing the substation connection to the external grid. The system operates at a nominal voltage of 23 kV. The single-line diagram is shown in Figure 4.

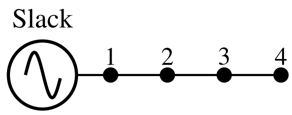

Figure 1. Single-line diagram of the 4-bus test system (radial configuration)

The corresponding three-phase impedance matrix for the lines are provided in Table 1. Load data and electrical parameters—including conductor type, characteristics, and line lengths— is given separately in Table 2.

Table 1. Impedance matrix for each conductor in 4 node system

Conductor	Impedance matrix		
1	$0.50250 + 0.30250i$	$0.02350 + 0.15160i$	$0.01718 + 0.20200i$
	$0.02350 + 0.15160i$	$0.50250 + 0.30250i$	$0.02020 + 0.10900i$
	$0.01718 + 0.20200i$	$0.02020 + 0.10900i$	$0.50250 + 0.30250i$
2	$0.40200 + 0.25100i$	$0.01520 + 0.12300i$	$0.03450 + 0.22400i$
	$0.01520 + 0.12300i$	$0.40200 + 0.25100i$	$0.09180 + 0.30100i$
	$0.03450 + 0.22400i$	$0.09180 + 0.30100i$	$0.40200 + 0.25100i$
3	$0.36600 + 0.18640i$	$0.03536 + 0.09980i$	$0.02450 + 0.08760i$
	$0.03536 + 0.09980i$	$0.36600 + 0.18640i$	$0.01560 + 0.07990i$
	$0.02450 + 0.08760i$	$0.01560 + 0.07990i$	$0.36600 + 0.18640i$

Table 2. Line data in 4-node system

Line	Node i	Node j	Conductor	Length (mi)	Line technology
1	1	2	1	0.6213	3Φ
2	2	3	2	0.6213	$2\Phi_{AB}$
3	3	4	3	0.6213	$1\Phi_{A}$

Table 3. Power per phase at node j

Node j	Phase A		Phase B		Phase C	
	P_j (kW)	Q_j (kvar)	P_j (kW)	Q_j (kvar)	P_j (kW)	Q_j (kvar)
2	1000	600	750	450	1250	750
3	1000	400	900	500	0	0
4	1000	500	0	0	0	0

The three-phase load of this system is connected in delta.

6.2. The 8-Bus Test System

The 8-bus system is a medium-scale unbalanced radial distribution network with 8 nodes, 7 lines, 7 load buses, and one slack bus. It operates at a nominal voltage of 11 kV. The system topology is illustrated in Figure 2

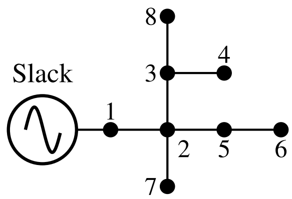

Figure 2. Single-line diagram of the test distribution system

The corresponding three-phase impedance matrix for the lines are provided in Table 3. Load data and electrical parameters—including conductor type, characteristics, and line lengths— is given separately in Table 4.

Table 4. Impedance matrix for each conductor in 8 node system

Conductor	Impedance matrix		
	$0.093654 + 0.040293i$	$0.031218 + 0.013431i$	$0.031218 + 0.013431i$
1	$0.031218 + 0.013431i$	$0.093654 + 0.040293i$	$0.031218 + 0.013431i$
	$0.031218 + 0.013431i$	$0.031218 + 0.013431i$	$0.093654 + 0.040293i$
	$0.15090 + 0.067155i$	$0.05203 + 0.022385i$	$0.05203 + 0.022385i$
2	$0.05203 + 0.022385i$	$0.15090 + 0.067155i$	$0.05203 + 0.022385i$
	$0.05203 + 0.022385i$	$0.05203 + 0.022385i$	$0.15090 + 0.067155i$
	$0.046827 + 0.020146i$	$0.015609 + 0.0067155i$	$0.015609 + 0.0067155i$
3	$0.015609 + 0.0067155i$	$0.046827 + 0.020146i$	$0.015609 + 0.0067155i$
	$0.015609 + 0.0067155i$	$0.015609 + 0.0067155i$	$0.046827 + 0.020146i$
	$0.031218 + 0.013431i$	$0.010406 + 0.004477i$	$0.010406 + 0.004477i$
4	$0.010406 + 0.004477i$	$0.031218 + 0.013431i$	$0.010406 + 0.004477i$
	$0.010406 + 0.004477i$	$0.010406 + 0.004477i$	$0.031218 + 0.013431i$
	$0.062436 + 0.026862i$	$0.020812 + 0.008954i$	$0.020812 + 0.008954i$
5	$0.020812 + 0.008954i$	$0.062436 + 0.026862i$	$0.020812 + 0.008954i$
	$0.020812 + 0.008954i$	$0.020812 + 0.008954i$	$0.062436 + 0.026862i$
	$0.078045 + 0.0335775i$	$0.026015 + 0.0111925i$	$0.026015 + 0.0111925i$
6	$0.026015 + 0.0111925i$	$0.078045 + 0.0335775i$	$0.026015 + 0.0111925i$
	$0.026015 + 0.0111925i$	$0.026015 + 0.0111925i$	$0.078045 + 0.0335775i$

Table 5. Line data in 8-node system

Line	**Node i**	**Node j**	**Conductor**	**Length (mi)**	**Line technology**
1	1	2	1	1	3Φ
2	2	3	2	1	$2\Phi_{BC}$
3	2	5	3	1	3Φ
4	2	7	3	1	$2\Phi_{BC}$
5	3	4	4	1	$1\Phi_C$
6	3	8	5	1	$1\Phi_B$
7	5	6	6	1	3Φ

Table 6. Power per phase at node j (8-node system)

Node j	**Phase A**		**Phase B**		**Phase C**	
	P_j (kW)	Q_j (kvar)	P_j (kW)	Q_j (kvar)	P_j (kW)	Q_j (kvar)
2	519	250	259	126	515	250
3	0	0	259	126	486	235
4	0	0	0	0	324	157
5	519	250	259	126	0	0
6	0	0	0	0	145	70
7	0	0	259	126	515	250
8	0	0	259	126	0	0

The three-phase loads of this system are connected in delta.

6.3. The 25-Bus Test System

The 25-bus system is a larger unbalanced radial distribution network consisting of 25 nodes, 24 lines, 22 load buses, and one slack bus. This system operates at a nominal voltage of 4.16 kV and is shown in Figure 3.

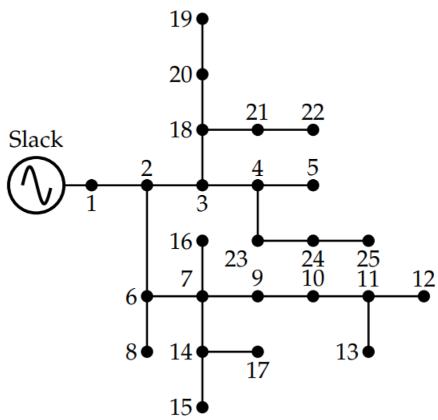

Figure 3. Single-line diagram of the 25-bus test system.

The corresponding three-phase impedance matrix for the lines are provided in Table 5. Load data and electrical parameters—including conductor type, characteristics, and line lengths— is given separately in Table 6.

Table 7. Impedance matrix for each conductor in 25 node system

Conductor	**Impedance matrix**		
1	$0.3686 + 0.6852i$	$0.0169 + 0.1515i$	$0.0155 + 0.1098i$
	$0.0169 + 0.1515i$	$0.3757 + 0.6715i$	$0.0188 + 0.2072i$
	$0.0155 + 0.1098i$	$0.0188 + 0.2072i$	$0.3723 + 0.6782i$
2	$0.9775 + 0.8717i$	$0.0167 + 0.1697i$	$0.0152 + 0.1264i$
	$0.0167 + 0.1697i$	$0.9844 + 0.8654i$	$0.0186 + 0.2275i$
	$0.0152 + 0.1264i$	$0.0186 + 0.2275i$	$0.981 + 0.8648i$
3	$1.928 + 1.4194i$	$0.0161 + 0.1183i$	$0.0161 + 0.1183i$
	$0.0161 + 0.1183i$	$1.9308 + 1.4215i$	$0.0161 + 0.1183i$
	$0.0161 + 0.1183i$	$0.0161 + 0.1183i$	$1.9337 + 1.4236i$

Table 8. Line data in 25-node system

Line	**Node i**	**Node j**	**Conductor**	**Length (mi)**	**Line technology**
1	1	2	1	0.1894	3Φ
2	2	3	1	0.0947	3Φ
3	2	4	2	0.0947	3Φ
4	4	5	2	0.0947	3Φ
5	5	6	2	0.0947	$1\Phi_A$
6	6	8	2	0.0947	$1\Phi_C$
7	8	9	2	0.1894	3Φ
8	9	10	2	0.0947	3Φ
9	10	11	2	0.0568	3Φ
10	11	12	3	0.0379	3Φ
11	11	13	3	0.0379	$1\Phi_C$
12	12	14	2	0.0379	$2\Phi_{AB}$
13	14	15	2	0.0568	$1\Phi_B$
14	14	16	3	0.0568	$2\Phi_{AB}$
15	16	17	3	0.0568	$1\Phi_B$
16	17	18	3	0.0568	$1\Phi_B$
17	18	19	2	0.0758	$2\Phi_{BC}$
18	19	20	2	0.0758	$2\Phi_{BC}$
19	20	21	3	0.0758	$1\Phi_B$
20	21	22	3	0.0758	$1\Phi_B$
21	22	23	3	0.0758	3Φ
22	23	24	2	0.0758	$2\Phi_{AB}$
23	24	25	3	0.0758	$1\Phi_A$

Table 9. Power per phase at node j (25-node system)

Node j	**Phase A**		**Phase B**		**Phase C**	
	P_j(kW)	Q_j(kvar)	P_j (kW)	Q_j (kvar)	P_j(kW)	Q_j(kvar)
2	0	0	0	0	0	0
3	36	21.6	28.8	19.2	42	26.4
4	57.6	43.2	4.8	3.4	48	30.0
5	43.2	28.8	28.8	19.2	36	24.0
6	43.2	28.8	0	0	0	0
8	0	0	0	0	3.6	2.4
9	72.0	50.4	38.4	28.8	48.0	30.0
10	36.0	21.6	28.8	19.2	32.0	26.4
11	50.4	31.7	24.0	14.4	36.0	24.0
12	57.6	36.0	48.0	33.6	48.0	36.0
13	0	0	0	0	36.0	24.0
14	57.6	36.0	38.4	28.8	0	0
15	0	0	4.8	2.9	0	0
16	57.6	4.3	31.8	28.8	0	0
17	0	0	33.6	24.0	0	0
18	0	0	38.4	28.8	0	0
19	0	0	4.8	3.4	6.0	4.8
20	0	0	38.4	28.8	54.0	38.4
21	0	0	3.4	2.4	0	0
22	0	0	57.6	43.2	0	0
23	8.6	64.8	4.8	3.8	60.0	4.2
24	50.4	36.0	43.2	30.7	0	0
25	8.6	6.5	0	0	0	0

The three-phase loads of this system are connected in star.

6.4. The 4-bus test system

The 4-bus system is a small-scale unbalanced radial distribution network comprising 4 nodes, 3 distribution lines, 3 load buses, and one slack bus representing the substation connection to the external grid. The system operates at a nominal voltage of 23 kV. The single-line diagram is shown in Figure 4.

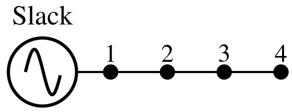

Figure 4. Single-line diagram of the 4-bus test system (radial configuration)

The corresponding three-phase impedance matrix for the lines are provided in Table 1. Load data and electrical parameters—including conductor type, characteristics, and line lengths— is given separately in Table 2.

Table 10. Impedance matrix for each conductor in 4 node system

Conductor	Impedance matrix		
1	$0.50250 + 0.30250i$	$0.02350 + 0.15160i$	$0.01718 + 0.20200i$
	$0.02350 + 0.15160i$	$0.50250 + 0.30250i$	$0.02020 + 0.10900i$
	$0.01718 + 0.20200i$	$0.02020 + 0.10900i$	$0.50250 + 0.30250i$
2	$0.40200 + 0.25100i$	$0.01520 + 0.12300i$	$0.03450 + 0.22400i$
	$0.01520 + 0.12300i$	$0.40200 + 0.25100i$	$0.09180 + 0.30100i$
	$0.03450 + 0.22400i$	$0.09180 + 0.30100i$	$0.40200 + 0.25100i$
3	$0.36600 + 0.18640i$	$0.03536 + 0.09980i$	$0.02450 + 0.08760i$
	$0.03536 + 0.09980i$	$0.36600 + 0.18640i$	$0.01560 + 0.07990i$
	$0.02450 + 0.08760i$	$0.01560 + 0.07990i$	$0.36600 + 0.18640i$

Table 11. Line data in 4-node system

Line	Node i	Node j	Conductor	Length (mi)	Line technology
1	1	2	1	0.6213	3Φ
2	2	3	2	0.6213	$2\Phi_{AB}$
3	3	4	3	0.6213	$1\Phi_{A}$

Table 12. Power per phase at node j

Node j	Phase A		Phase B		Phase C	
	P_j (kW)	Q_j (kvar)	P_j (kW)	Q_j (kvar)	P_j (kW)	Q_j (kvar)
2	1000	600	750	450	1250	750
3	1000	400	900	500	0	0
4	1000	500	0	0	0	0

The three-phase load of this system is connected in delta.

7. Results and discussion

This section presents the numerical validation of the proposed fixed-point power flow methodology for unbalanced distribution systems. To assess accuracy, computational performance, and scalability, the algorithm was implemented in MATLAB® and benchmarked against the industry-standard software DIgSILENT PowerFactory®. The validation employs three test systems of increasing complexity—4, 8, 25 and 124 nodes—each featuring mixed single-phase, two-phase, and three-phase laterals. For each system, a comparative analysis of voltage profiles and system-wide power balance is provided, alongside a detailed evaluation of the algorithm's convergence behavior and execution time. The computational environment and convergence criteria used for all simulations are first specified to ensure reproducibility.

7.1. Computational specifications

All simulations and model compilations were performed using DIgSILENT PowerFactory 2021, while the proposed methodology was implemented in MATLAB R2023a. The computations were executed on a laptop with the following specifications:

- **Processor:** Intel(R) Core(TM) i7-10200U CPU @ 4 GHz
- **Memory:** 16 GB RAM
- **Operating System:** Windows 11 (64-bit architecture)

A convergence tolerance of $\varepsilon = 1 \times 10^{-10}$ and a maximum of 100 iterations were configured for the solvers in both software environments.

7.2. Four-Node test system validation

The proposed fixed-point formulation was validated using a balanced four-node test system by comparing its results with those obtained from the commercial power system analysis software DIgSILENT PowerFactory®. The comparative analysis focuses on nodal voltages and system-wide power balance.

7.2.1. Voltage profile comparison Table 13 presents a phase-by-phase comparison of the steady-state voltage phasors obtained from the MATLAB® implementation and the PowerFactory reference solution. The results demonstrate excellent agreement in both magnitude and phase angle across all nodes and phases, with maximum deviations on the order of 10^{-3} p.u. for magnitudes and $0.05°$ for angles.

Table 13. Comparison of voltage phasors between MATLAB® and DIgSILENT® for the four-node system.

Node	**MATLAB®**						**DIgSILENT®**					
	V_a (p.u.)	θ_a (°)	V_b (p.u.)	θ_b (°)	V_c (p.u.)	θ_c (°)	V_a (p.u.)	θ_a (°)	V_b (p.u.)	θ_b (°)	V_c (p.u.)	θ_c (°)
1	1.000000	0.0000	1.000000	-120.0000	1.000000	120.0000	0.999830	-0.0244	1.000256	-119.9868	0.999914	120.0112
2	0.996812	-0.0140	0.996822	-119.9653	0.998333	120.0382	0.996484	-0.0095	0.998648	-119.9335	0.998913	120.0546
3	0.995810	-0.0194	0.998954	-119.9662	0.998133	120.0633	0.995482	-0.0150	0.998448	-119.9345	0.999176	120.0797
4	0.996205	-0.0335	0.998190	-119.9479	0.998311	120.0402	0.995683	-0.0179	0.998648	-119.9028	0.998422	120.0546

7.2.2. Power balance analysis The system-wide power balance is summarized in Table 14. Both the total generation and the resulting network losses calculated by the proposed method show negligible deviation from the PowerFactory benchmark, with relative differences below 0.01% for active power and reactive power quantities.

Table 14. System power balance comparison between MATLAB® and PowerFactory®.

Quantity	**MATLAB®**		**PowerFactory®**	
	Active (kW)	**Reactive (kvar)**	**Active (kW)**	**Reactive (kvar)**
Generation	5921.80	3208.40	5921.77	3208.41
Load	5900.00	3200.00	5900.00	3200.00
Losses	21.77	8.41	21.78	8.41

7.2.3. Computational performance The fixed-point method converged to the specified tolerance of $\varepsilon = 1 \times 10^{-10}$ in only 4 iterations, requiring a total execution time of 0.0195 seconds. This demonstrates both the numerical robustness and computational efficiency of the proposed formulation for small-scale systems.

7.3. Eight-node test system validation

To further validate the proposed methodology, the fixed-point formulation was applied to an eight-node balanced test system and the results were compared with the DIgSILENT PowerFactory® benchmark.

7.3.1. Voltage profile comparison Table 15 presents the detailed comparison of voltage phasors across all eight nodes. The results from MATLAB® and PowerFactory show strong agreement, with voltage magnitude deviations consistently below 5×10^{-4} p.u. and phase angle differences within $0.02°$. The consistent alignment across all three phases confirms the accuracy of the fixed-point formulation for larger networks.

Table 15. Comparison of voltage phasors between MATLAB® and DIgSILENT® for the eight-node system.

Node	MATLAB®						DIgSILENT®					
	V_a (p.u.)	θ_a (°)	V_b (p.u.)	θ_b (°)	V_c (p.u.)	θ_c (°)	V_a (p.u.)	θ_a (°)	V_b (p.u.)	θ_b (°)	V_c (p.u.)	θ_c (°)
1	1.000000	0.000000	1.000000	-120.000000	1.000000	120.000000	1.000031	0.002858	1.000024	-119.994756	0.999945	119.991898
2	0.999500	-0.005121	0.999487	-119.991009	0.998890	119.988184	0.999513	-0.006045	0.999559	-119.980088	0.998752	119.991666
3	0.999872	-0.007061	0.998813	-119.977963	0.997888	119.958122	0.999855	-0.014285	0.998966	-119.957574	0.997613	119.980951
4	0.999887	-0.008780	0.998831	-119.976332	0.997787	119.958384	0.999870	-0.016004	0.998984	-119.955942	0.997511	119.981212
5	0.999527	-0.008066	0.999518	-119.988208	0.998716	119.988614	0.999539	-0.008990	0.999590	-119.977287	0.998578	119.992097
6	0.999544	-0.009984	0.999538	-119.986384	0.998603	119.988897	0.999557	-0.010908	0.999611	-119.975463	0.998465	119.992379
7	0.999273	-0.004546	0.999522	-119.994868	0.998930	119.991853	0.999285	-0.005469	0.999604	-119.991915	0.998908	119.999828
8	0.999901	-0.004374	0.998646	-119.977545	0.997914	119.955292	0.999884	-0.011597	0.998799	-119.957156	0.997638	119.978120

7.3.2. Power balance analysis The system-wide power balance for the eight-node system is presented in Table 16. The proposed methodology demonstrates excellent agreement with the commercial software, with generation and loss values showing relative errors below 0.05%. The consistent matching of both active and reactive power components validates the formulation's ability to accurately model power flow in medium-sized networks.

Table 16. System power balance comparison between MATLAB® and PowerFactory® for the eight-node system.

Quantity	MATLAB®		PowerFactory®	
	Active (kW)	Reactive (kvar)	Active (kW)	Reactive (kvar)
Generation	4336.10	2099.80	4336.21	2099.84
Load	4318.00	2092.00	4318.00	2092.00
Losses	18.06	7.84	18.21	7.84

7.3.3. Computational performance The fixed-point method maintained its computational efficiency for the larger system, converging to the specified tolerance of $\varepsilon = 1 \times 10^{-10}$ in 4 iterations. The total execution time was 0.0295 seconds, representing only a 51% increase in computational time compared to the four-node system despite the doubled network size.

7.4. Twenty-Five-Node Test System Validation

To comprehensively assess the performance of the fixed-point methodology on a larger distribution network, a twenty-five-node test system was analyzed and validated against the DIgSILENT PowerFactory® reference solution.

7.4.1. Voltage profile comparison Table 17 presents the detailed voltage phasor comparison for all twenty-five nodes. The fixed-point formulation demonstrates remarkable accuracy, with voltage magnitude deviations consistently below 2×10^{-3} p.u. and phase angle differences within $0.01°$ across the entire network. This close alignment confirms the method's robustness in handling larger-scale systems with more complex voltage profiles.

Table 17. Comparison of voltage phasors between MATLAB® and DIgSILENT® for the twenty-five-node system.

Node	MATLAB®						DIgSILENT®					
	V_a (p.u.)	θ_a (°)	V_b (p.u.)	θ_b (°)	V_c (p.u.)	θ_c (°)	V_a (p.u.)	θ_a (°)	V_b (p.u.)	θ_b (°)	V_c (p.u.)	θ_c (°)
1	1.0000	-0.003	1.0000	-119.990	1.0000	119.990	0.99999	-0.002	0.99997	-119.990	1.00004	120.000
2	0.9929	-0.546	0.9933	-120.170	0.9955	119.470	0.99290	-0.546	0.99324	-120.170	0.99549	119.470
3	0.9914	-0.659	0.9918	-120.180	0.9945	119.340	0.99116	-0.659	0.99175	-120.180	0.99444	119.340
4	0.9906	-0.709	0.9910	-120.170	0.9940	119.280	0.99036	-0.709	0.99113	-120.170	0.99406	119.280
5	0.9901	-0.715	0.9907	-120.170	0.9938	119.270	0.99004	-0.715	0.99083	-120.170	0.99383	119.270
6	0.9888	-0.635	0.9896	-120.100	0.9926	119.420	0.98924	-0.635	0.98963	-120.100	0.99279	119.420
7	0.9856	-0.708	0.9865	-120.030	0.9903	119.360	0.98607	-0.708	0.98663	-120.030	0.99046	119.360
8	0.9878	-0.671	0.9894	-120.080	0.9920	119.440	0.98887	-0.671	0.98906	-120.080	0.99257	119.440
9	0.9842	-0.762	0.9850	-120.000	0.9893	119.330	0.98420	-0.762	0.98479	-120.000	0.98908	119.330
10	0.9827	-0.800	0.9835	-119.990	0.9883	119.310	0.98282	-0.800	0.98340	-119.990	0.98801	119.310
11	0.9819	-0.823	0.9828	-119.980	0.9877	119.290	0.98216	-0.823	0.98273	-119.980	0.98751	119.290
12	0.9816	-0.826	0.9825	-119.980	0.9874	119.300	0.98184	-0.826	0.98240	-119.980	0.98720	119.300
13	0.9817	-0.839	0.9825	-119.980	0.9876	119.290	0.98191	-0.839	0.98244	-119.980	0.98729	119.290
14	0.9847	-0.714	0.9855	-120.010	0.9896	119.330	0.98507	-0.714	0.98580	-120.010	0.98972	119.330
15	0.9845	-0.715	0.9853	-120.010	0.9894	119.330	0.98504	-0.715	0.98577	-120.010	0.98970	119.330
16	0.9852	-0.723	0.9860	-120.030	0.9899	119.360	0.98576	-0.723	0.98630	-120.030	0.99026	119.360
17	0.9843	-0.714	0.9851	-119.990	0.9892	119.330	0.98453	-0.714	0.98537	-119.990	0.98931	119.330
18	0.9903	-0.666	0.9909	-120.150	0.9937	119.320	0.98962	-0.666	0.99034	-120.150	0.99322	119.320
19	0.9889	-0.667	0.9896	-120.130	0.9924	119.310	0.98903	-0.667	0.98983	-120.130	0.99276	119.310
20	0.9894	-0.666	0.9902	-120.140	0.9930	119.310	0.98912	-0.666	0.98991	-120.140	0.99283	119.310
21	0.9899	-0.666	0.9908	-120.130	0.9936	119.320	0.98872	-0.666	0.98946	-120.130	0.99240	119.320
22	0.9898	-0.666	0.9907	-120.120	0.9935	119.330	0.98789	-0.666	0.98863	-120.120	0.99163	119.330
23	0.9899	-0.697	0.9902	-120.130	0.9934	119.270	0.98974	-0.697	0.99071	-120.130	0.99369	119.270
24	0.9897	-0.713	0.9899	-120.130	0.9933	119.280	0.98951	-0.713	0.99036	-120.130	0.99352	119.280
25	0.9896	-0.714	0.9898	-120.120	0.9932	119.270	0.98941	-0.714	0.99028	-120.120	0.99345	119.270

7.4.2. Power balance analysis Table 18 summarizes the system-wide power balance for the twenty-five-node network. The results demonstrate exceptional agreement, with generation values showing relative errors below 0.015% and loss calculations matching within 0.2%. The consistent accuracy across all power components reinforces the reliability of the fixed-point formulation for practical distribution system analysis.

Table 18. System power balance comparison between MATLAB® and PowerFactory® for the twenty-five-node system.

Quantity	**MATLAB®**		**PowerFactory®**	
	Active (kW)	**Reactive (kvar)**	**Active (kW)**	**Reactive (kvar)**
Generation	1511.90	1093.40	1511.88	1093.40
Load	1501.20	1081.50	1501.20	1081.50
Losses	10.66	11.88	10.68	11.90

7.4.3. Computational performance The fixed-point method maintained consistent convergence behavior for the twenty-five-node system, reaching the specified tolerance of $\varepsilon = 1 \times 10^{-10}$ in only 4 iterations. The total execution time was 0.0479 seconds, demonstrating excellent scalability with a computational time increase of only 62% compared to the eight-node system despite the network size tripling.

7.5. Simulation of systems with increased active power load

In the following section, systems with the same topology as the previously analyzed 4-, 8-, and 25-node networks will be presented, but assuming a tenfold increase in active power demand. This is done in order to analyze the behavior of the algorithm as the loading level increases, since when using a fixed-point methodology, the convergence of the method depends on the mapping being contractive. This condition is guaranteed when the Jacobian of the voltage function remains between 0 and 1, and this Jacobian grows as the load current increases.

For values greater than 1, the method diverges, which allows the increase in current magnitude to be directly related to the convergence limits of the proposed method.

7.6. Validation of the Four-Node Test System Under a Tenfold Increase in Resistive Load

Following the approach of the previous section, the previously described 4-node system is simulated with a tenfold increase in resistive load in order to further evaluate the proposed methodology and algorithm.

7.6.1. Voltage profile comparison Table 19 presents a detailed comparison of the voltage phasor for the four nodes, with maximum voltage magnitude deviations of 0.001037 p.u. and maximum phase angle differences of 0.23° across the entire network. This increase in voltage profile variation compared to systems with less load is due to the fact that an increase in load generates greater voltage variations.

Table 19. Comparison of voltage phasors between MATLAB® and DIgSILENT® for the four-node system.

Node	MATLAB®						DIgSILENT®					
	V_a (p.u.)	θ_a (°)	V_b (p.u.)	θ_b (°)	V_c (p.u.)	θ_c (°)	V_a (p.u.)	θ_a (°)	V_b (p.u.)	θ_b (°)	V_c (p.u.)	θ_c (°)
1	1.000000	0.000000	1.000000	-120.000000	1.000000	120.000000	0.999076	-0.228218	0.999901	-119.955978	1.001037	120.183799
2	0.967205	-0.606672	0.989190	-120.266309	0.984755	120.131936	0.966258	-0.838971	0.989101	-120.223370	0.985817	120.320655
3	0.948974	-1.076062	0.986691	-120.398279	0.984755	120.131936	0.948003	-1.309850	0.986613	-120.356576	0.985817	120.320655
4	0.941431	-1.279856	0.986691	-120.398279	0.984755	120.131936	0.940453	-1.514066	0.986613	-120.356576	0.985817	120.320655

7.6.2. Power balance analysis Table 20 summarizes the system-wide power balance for the four-node network. The results demonstrate exceptional agreement, with generation values showing relative errors below 0.0451% and loss calculations matching within 0.2431%.

Table 20. System power balance comparison between MATLAB® and DIgSILENT PowerFactory® for the four-node system.

Quantity	MATLAB®		DIgSILENT PowerFactory®	
	Active (kW)	Reactive (kvar)	Active (kW)	Reactive (kvar)
Generation	60859.00	3942.70	60860.00	3944.48
Load	59000.00	3200.00	59000.00	3200.00
Losses	1858.60	742.67	1860.00	744.48

7.6.3. Computational performance The fixed-point method maintained consistent convergence for the 4-node system as the load increased, reaching the specified tolerance of $\epsilon = 1 \times 10^{-10}$ in 6 iterations. This means that it required 2 additional iterations compared to the same system under a lower loading condition. The convergence time was 0.029906 seconds, representing an increase of 0.010406 seconds.

7.7. Validation of the Eight-Node Test System Under a Tenfold Increase in Resistive Load

Following the approach of the previous section, the previously described 8-node system is simulated with a tenfold increase in resistive load in order to further evaluate the proposed methodology and algorithm.

7.7.1. Voltage profile comparison Table 21presents a detailed comparison of the voltage phasors for the eight-node system, showing maximum voltage magnitude deviations of 0.000211 p.u. and maximum phase angle differences of 0.105028° across the network. As observed in the previous case, the increase in load also produced a considerable variation in the voltage profile.

Table 21. Comparison of voltage phasors between MATLAB® and DIgSILENT® for the eight-node system.

Node	MATLAB®						DIgSILENT®					
	V_a (p.u.)	θ_a (°)	V_b (p.u.)	θ_b (°)	V_c (p.u.)	θ_c (°)	V_a (p.u.)	θ_a (°)	V_b (p.u.)	θ_b (°)	V_c (p.u.)	θ_c (°)
1	1.000000	0.000000	1.000000	-120.000000	1.000000	120.000000	1.000222	0.077301	0.999780	-119.995170	1.000001	119.917852
2	0.996839	-0.135140	0.991360	-120.015182	0.988772	119.658594	0.997056	-0.058090	0.991145	-120.010380	0.988774	119.576458
3	0.996839	-0.135140	0.985343	-119.945013	0.980145	119.332198	0.997056	-0.058090	0.985133	-119.940290	0.980149	119.250213
4	0.996839	-0.135140	0.985343	-119.945013	0.979274	119.313148	0.997293	-0.069591	0.985189	-119.922550	0.979278	119.231163
5	0.994997	-0.166203	0.990927	-120.052745	0.988595	119.674497	0.995215	-0.089162	0.990713	-120.047920	0.988595	119.592393
6	0.995262	-0.178845	0.990986	-120.033144	0.987629	119.653535	0.995479	-0.101843	0.990772	-120.028320	0.987629	119.571430
7	0.996839	-0.135140	0.990453	-119.995732	0.986996	119.600495	0.997056	-0.058090	0.990239	-119.990950	0.986997	119.518381
8	0.996839	-0.135140	0.983957	-119.975149	0.980145	119.332198	0.997137	-0.030112	0.983746	-119.970440	0.980534	119.232170

7.7.2. Power balance analysis Table 22 shows that the generated power error does not exceed 0.003033% and that the loss error does not exceed 0.013917%, which remain highly acceptable values when comparing the MATLAB® algorithm with DIgSILENT®.This continues to show the validity of the algorithm even when there are heavy loads.

Table 22. System power balance comparison between MATLAB® and DIgSILENT PowerFactory® for the eight-node system.

Quantity	MATLAB®		DIgSILENT PowerFactory®	
	Active (kW)	Reactive (kvar)	Active (kW)	Reactive (kvar)
Generation	43677.00	2307.60	43676.84	2307.53
Load	43180.00	2092.00	43180.00	2092.00
Losses	496.90	215.56	496.84	215.53

7.7.3. Computational performance The fixed-point method showed that the system maintained consistent convergence for the 8-node system as the load increased, reaching the specified tolerance of $\epsilon = 1 \times 10^{-10}$ in 5 iterations. This means that it required one additional iteration compared to the same system under lower loading conditions. The convergence time was 0.036180 seconds, representing an increase of 0.00668 seconds compared to the convergence time obtained for the same system under lower load conditions.

7.8. Validation of the Twenty-Five-Node Test System Under a Tenfold Increase in Resistive Load

Following the same approach described in the previous sections, the previously presented 25-node system is simulated under a tenfold increase in resistive load conditions in order to further evaluate the robustness, convergence performance, and computational behavior of the proposed methodology and algorithm under highly stressed operating scenarios.

7.8.1. Voltage profile comparison Table 23 presents the comparison of voltage magnitudes and phase angles obtained from both software tools under a tenfold increase in the resistive load at each node of the system. The results show that the maximum voltage magnitude deviation was only 4.03×10^{-4} p.u., while the largest angular difference reached just $0.0163°$ between MATLAB® and DIgSILENT®. These minimal discrepancies demonstrate that the proposed methodology remains accurate and robust even under highly stressed operating conditions in the distribution system.

Table 23. Comparison of voltage phasors between MATLAB® and DIgSILENT® for the twenty-five-node system.

Node	MATLAB®						DIgSILENT®					
	V_a (p.u.)	θ_a (°)	V_b (p.u.)	θ_b (°)	V_c (p.u.)	θ_c (°)	V_a (p.u.)	θ_a (°)	V_b (p.u.)	θ_b (°)	V_c (p.u.)	θ_c (°)
1	1.000000	0.0000	1.000000	-120.0000	1.000000	120.0000	0.999910	-0.0152	1.000019	-119.9978	1.000072	120.0130
2	0.968250	-2.1002	0.976216	-121.5343	0.983558	118.6395	0.968153	-2.1158	0.976236	-121.5323	0.983635	118.6528
3	0.962864	-2.4337	0.969487	-121.9400	0.979628	118.2297	0.962766	-2.4494	0.969508	-121.9381	0.979705	118.2430
4	0.958885	-2.7597	0.967631	-122.0284	0.976380	117.9853	0.958786	-2.7754	0.967652	-122.0265	0.976458	117.9988
5	0.956348	-2.8631	0.965966	-122.0802	0.974390	117.9108	0.956248	-2.8789	0.965987	-122.0783	0.974469	117.9243
6	0.944147	-3.0320	0.962412	-122.0205	0.971998	118.2840	0.944095	-3.0478	0.962434	-122.0186	0.972077	118.2974
7	0.922842	-3.8848	0.948314	-122.5315	0.960924	117.9170	0.922738	-3.9008	0.948337	-122.5296	0.961005	117.9305
8	0.944195	-3.0309	0.962339	-122.0171	0.971577	118.2649	0.944094	-3.0467	0.962361	-122.0152	0.971655	118.2783
9	0.909456	-4.4519	0.939806	-122.7788	0.949208	117.4766	0.909349	-4.4681	0.939829	-122.7770	0.949290	117.4903
10	0.900605	-4.8350	0.933455	-122.9598	0.940329	117.1282	0.900497	-4.8512	0.933478	-122.9581	0.940413	117.1419
11	0.896667	-5.0098	0.930690	-123.0341	0.936102	116.9577	0.896559	-5.0260	0.930714	-123.0324	0.936186	116.9715
12	0.893842	-5.1184	0.928452	-123.1153	0.933810	116.8793	0.893733	-5.1347	0.928476	-123.1135	0.933894	116.8911
13	0.896667	-5.0098	0.930690	-123.0341	0.934390	116.8909	0.896559	-5.0260	0.930714	-123.0324	0.934474	116.9046
14	0.918703	-4.0280	0.944192	-122.7332	0.960924	117.9170	0.918598	-4.0441	0.944215	-122.7313	0.961005	117.9305
15	0.918703	-4.0280	0.944019	-122.7414	0.960924	117.9170	0.918598	-4.0441	0.944042	-122.7395	0.961005	117.9305
16	0.919221	-4.0564	0.946900	-122.6041	0.960924	117.9170	0.919116	-4.0725	0.946923	-122.6023	0.961005	117.9305
17	0.918703	-4.0280	0.941811	-122.8244	0.960924	117.9170	0.918598	-4.0441	0.941834	-122.8225	0.961005	117.9305
18	0.962864	-2.4337	0.960268	-122.2924	0.978339	118.1120	0.962766	-2.4494	0.960289	-122.2904	0.977936	118.1254
19	0.962864	-2.4337	0.956601	-122.3961	0.974342	117.9473	0.962766	-2.4494	0.956622	-122.3942	0.974421	117.9607
20	0.962864	-2.4337	0.957072	-122.3805	0.974870	117.9670	0.962766	-2.4494	0.957093	-122.3786	0.974948	117.9804
21	0.962864	-2.4337	0.954516	-122.5057	0.978339	118.1120	0.962766	-2.4494	0.954537	-122.5037	0.977936	118.1254
22	0.962864	-2.4337	0.949094	-122.7094	0.978339	118.1120	0.962766	-2.4494	0.949115	-122.7075	0.977936	118.1254
23	0.955445	-2.8714	0.965383	-122.1001	0.973759	117.8870	0.955345	-2.8872	0.965404	-122.0982	0.973837	117.9004
24	0.952358	-2.9892	0.963766	-122.1836	0.973759	117.8870	0.952258	-3.0049	0.963787	-122.1820	0.973837	117.9004
25	0.951553	-3.0195	0.963766	-122.1836	0.973759	117.8870	0.951452	-3.0353	0.963787	-122.1820	0.973837	117.9004

7.8.2. Power balance analysis Table 24 presents the power balance obtained from each software package, demonstrating the agreement between both systems and, consequently, the robustness of the proposed methodology under particular loading conditions. The relative errors do not exceed 0.01%, which provides quantitative evidence of the performance of the methodology under stressed operating conditions.

Table 24. System power balance comparison between MATLAB® and DIgSILENT PowerFactory® for the twenty-five-node system.

Quantity	MATLAB®		DIgSILENT PowerFactory®	
	Active (kW)	**Reactive (kvar)**	**Active (kW)**	**Reactive (kvar)**
Generation	16128.00	1998.10	16128.33	1998.16
Load	15292.00	1081.50	15292.00	1081.50
Losses	836.29	916.58	836.33	916.66

7.8.3. Computational performance The proposed methodology showed agreement in the obtained results and maintained satisfactory convergence performance, requiring 8 iterations, which is 4 more than the case without the load particularity. The total execution time for this case was 0.068872 s, representing a 43% increase compared to the base load case. All simulations were performed under the same error tolerance previously specified.

7.9. Comprehensive analysis of results

A rigorous, multi-scale validation confirms the proposed fixed-point methodology's exceptional accuracy in solving unbalanced power flows for distribution networks with mixed-phase laterals. The voltage phasors computed by the MATLAB® implementation exhibit remarkable agreement with the DIgSILENT PowerFactory® benchmark across all test systems. Deviations in voltage magnitude remain within the order of 10^{-3} to 10^{-4} per unit, while phase angle differences are consistently less than $0.05°$. This precision extends to system-wide power balance, where total generation, load, and technical losses show relative errors below 0.05%. These results validate the mathematical formulation's ability to accurately capture the electrical behavior of complex, unbalanced networks, particularly through its correct handling of wye and delta load connections and the construction of the three-phase nodal admittance matrix.

Equally notable is the algorithm's computational performance. The method demonstrated robust and rapid convergence, reaching the stringent tolerance of $\varepsilon = 1 \times 10^{-10}$ in only four iterations for all test cases. The execution times were 0.0195 s, 0.0295 s, and 0.0479 s for the 4-, 8-, and 25-node systems, respectively, revealing near-linear scalability and high computational efficiency. This combination of numerical accuracy, deterministic convergence, and low execution cost establishes the proposed fixed-point method as a highly effective tool for analyzing real-world distribution networks. It is particularly well-suited for the radial topologies, inherent phase unbalance, and mixed load configurations that often challenge conventional power flow solvers.

7.9.1. Proposed methodology under stressed conditions In order to subject the proposed methodology to stressed operating conditions, a tenfold increase in active power demand was applied to the previously presented 4-, 8-, and 25-node systems. The following tables summarize the comparative computational performance obtained in MATLAB® for both loading scenarios.

Table 25. Computational performance comparison for the four-node system under base and stressed loading conditions.

ITEM	BASE CASE	X10 CASE	ABSOLUTE DIFFERENCE
Maximum voltage error (p.u.)	0.001	0.001037	0.000037
Maximum angle error (°)	0.05	0.23	0.18
Iterations	4	6	2
Execution time (s)	0.0195	0.029906	0.010406

Table 26. Computational performance comparison for the eight-node system under base and stressed loading conditions.

ITEM	BASE CASE	X10 CASE	ABSOLUTE DIFFERENCE
Maximum voltage error (p.u.)	0.0005	0.000211	0.000289
Maximum angle error (°)	0.02	0.105028	0.085028
Iterations	4	5	1
Execution time (s)	0.029500	0.036180	0.006680

Table 27. Computational performance comparison for the twenty-five-node system under base and stressed loading conditions.

ITEM	BASE CASE	X10 CASE	ABSOLUTE DIFFERENCE
Maximum voltage error (p.u.)	0.002	0.000403	0.001597
Maximum angle error (°)	0.01	0.016300	0.006300
Iterations	4	8	4
Execution time (s)	0.047900	0.068872	0.020972

Table 28. General convergence behavior of the proposed methodology under stressed loading conditions.

SYSTEM	ADDITIONAL ITERATIONS	EXECUTION TIME INCREASE (%)
Four-node system	2	53.36
Eight-node system	1	22.64
Twenty-five-node system	4	43.78

The obtained results allow concluding that the proposed fixed-point formulation exhibits robust, stable, and consistent behavior even under severely stressed loading conditions. By increasing the active power demand by a factor of ten in the analyzed systems, the methodology maintained convergence in all evaluated cases, demonstrating that the proposed iterative mapping remains contractive even under highly stressed operating scenarios.

The load increase produced larger voltage profile variations and an increase in the number of iterations required to reach the specified tolerance. This behavior is consistent with fixed-point theory, since the increase in load current causes the derivative of the iterative operator to approach unity, thereby reducing the convergence speed of the algorithm. Nevertheless, despite these unfavorable conditions, the methodology preserved numerical stability and successfully converged for all analyzed systems.

Additionally, the errors obtained between MATLAB and DIgSILENT PowerFactory remained extremely low in terms of voltage magnitude, phase angle, and power balance, even under stressed loading conditions. This demonstrates that the accuracy of the formulation does not significantly deteriorate under severe load increases and confirms the capability of the methodology to accurately represent the electrical behavior of the system.

Finally, although the computational time and the number of iterations increased with respect to the base cases, the observed growth remained moderate and controlled, demonstrating good computational scalability. Overall, these results validate the robustness, accuracy, and convergence capability of the proposed methodology for power flow analysis in distribution networks under both normal and highly demanding operating conditions.

8. Conclusions and future works

This paper presented a fixed-point methodology for unbalanced power flow analysis in three-phase distribution networks with mixed single-phase, two-phase, and three-phase laterals. The formulation incorporates detailed models for wye and delta load connections and employs a per-unit, impedance-based iterative scheme to compute nodal voltages. The proposed algorithm was implemented in MATLAB and rigorously validated against the industry-standard software DIgSILENT PowerFactory using three test systems of varying scale and complexity.

The results conclusively demonstrate that the method achieves high numerical accuracy, with voltage and power mismatches negligible for practical engineering purposes. Its consistent 4-iteration convergence and low computational time highlight the algorithm's efficiency and robustness, making it suitable for planning, operational analysis, and repeated simulations in distribution networks. By successfully addressing the challenges of phase unbalance and mixed topologies, this work provides a reliable and accessible computational tool that bridges the gap between academic research and industrial application in distribution system analysis.

Additional stress-condition analyses were carried out by increasing the active power demand of the evaluated systems by a factor of ten in order to assess the convergence limits and numerical robustness of the proposed fixed-point formulation under highly demanding operating conditions. The results demonstrated that the methodology maintained convergence in all analyzed cases despite the increase in voltage deviations, iteration count, and computational time. This behavior is consistent with fixed-point theory, since the increase in load current causes the derivative of the iterative operator to approach unity, thereby reducing the convergence rate of the algorithm. Nevertheless, the methodology preserved high numerical accuracy and stable convergence behavior, with very low discrepancies compared to DIgSILENT PowerFactory, confirming the robustness and reliability of the proposed approach even under stressed loading conditions.

Such as photovoltaic generation and battery energy storage systems, modeled as voltage-dependent or current-dependent injection sources. Future work will also explore the integration of additional distributed energy resources (DER), including electric vehicles, microgrids, and control strategies associated with power electronic converters.

Likewise, the incorporation of voltage regulation devices, including on-load tap changers and step voltage regulators, within the fixed-point formulation will be investigated. Similarly, the applicability of the methodology to more complex distribution configurations, such as open-delta systems and networks with different multiphase connection schemes, will be evaluated.

The scalability of the algorithm will be tested on large real-world distribution feeders with thousands of nodes. Finally, the development of a user-friendly graphical interface or its integration into open-source distribution system analysis platforms is expected to improve the practical adoption of the tool by utility engineers and researchers.

REFERENCES

1. Olena Chygryn, Yevheniia Ziabina, Dalia Štreimikienė, and Yuriy Bilan. Outcomes of innovative technologies and smart transformation of the energy sector. *Journal of Innovation & Knowledge*, 12:100910, March 2026.
2. Jean Paul A. Yaacoub, Hassan N. Noura, Ola Salman, and Khaled Chahine. Toward secure smart grid systems: Risks, threats, challenges, and future directions. *Future Internet*, 17(7):318, July 2025.
3. C.G. Marcelino, V. Torres, L. Carvalho, M. Matos, and V. Miranda. Multi-objective identification of critical distribution network assets in large interruption datasets. *International Journal of Electrical Power & Energy Systems*, 137:107747, May 2022.
4. Rodrigo Moreno, Bernardo Bezerra, Hugh Rudnick, Carlos Suazo-Martinez, Martha Carvalho, Alejandro Navarro, Carlos Silva, and Goran Strbac. Distribution Network Rate Making in Latin America: An Evolving Landscape. *IEEE Power and Energy Magazine*, 18(3):33–48, May 2020.
5. Oscar Gómez Carmona, Mauricio Granada Echeverri, and Carlos Julio Zapata Grisales. *Technical losses in secondary electrical power distribution networks (In Spanish)*. Universidad Tecnológica de Pereira, 2020.
6. Obed Renato Jiménez Meza, Paz Vicente Cantú Gutiérrez, and Jorge Luis Arizpe Islas. Technical energy losses in a distribution power grid (In Spanish). *Multidisciplinas de la Ingeniería*, 9(13):01–11, December 2023.
7. Hiroki Kojima, Koki Fukaya, Naoki Hayakawa, Masahiro Hanai, and Hitoshi Okubo. Power Flow Control and Maintenance Strategy of Transformers in Transmission and Distribution Systems. *IEEJ Transactions on Power and Energy*, 135(5):316–321, 2015.
8. Jiawei Zhang, Frederik Geth, Rahmat Heidari, and Gregor Verbič. Beyond simplifications: Evaluating assumptions for low-voltage network modelling in the DER era. *Sustainable Energy, Grids and Networks*, 43:101860, September 2025.
9. Brandon Cortés-Caicedo, Oscar Danilo Montoya, Luis Fernando Grisales-Noreña, Santiago Bustamante-Mesa, and Carlos Andrés Torres-Pinzón. Joint Feeder Routing and Conductor Sizing in Rural Unbalanced Three-Phase Distribution Networks: An Exact Optimization Approach. *Sci*, 7(4):165, November 2025.
10. Brandon Cortés-Caicedo, Oscar Danilo Montoya, Luis Fernando Grisales-Noreña, Walter Gil-González, and Jesús C. Hernández. Simultaneous Feeder Routing and Conductor Sizing for System Cost Reduction in Rural Distribution Networks: A Cascade Metaheuristic Approach. *IEEE Access*, 13:201310–201334, 2025.
11. Le Nam Hai Pham, Jose Miguel Riquelme-Dominguez, and Francisco Gonzalez-Longatt. Exploring data-driven technique in optimal power flow study through real-time cyber-physical power system under uncertainties. *Energy*, 332:137091, September 2025.
12. Ahmed Babiker, Sulaiman S. Ahmad, Ijaz Ahmed, Muhammad Khalid, Mohammad A. Abido, and Fahad Saleh Al-Ismail. Optimal Power Flow: A Review of State-of-the-Art Techniques and Future Perspectives. *IEEE Access*, 13:60012–60039, 2025.
13. B. Hammer, C. Fuhr, J. Hanson, and U. Konigorski. Differences of Power Flows in Transmission and Distribution Networks and Implications on Inverter Droop Control. In *2019 International Conference on Clean Electrical Power (ICCEP)*, pages 46–54. IEEE, July 2019.
14. Jen-Hao Teng and Chuo-Yean Chang. Backward/Forward Sweep-Based Harmonic Analysis Method for Distribution Systems. *IEEE Transactions on Power Delivery*, 22(3):1665–1672, July 2007.
15. Oscar Danilo Montoya and Walter Gil-González. On the numerical analysis based on successive approximations for power flow problems in ac distribution systems. *Electric Power Systems Research*, 187:106454, October 2020.
16. Oscar Danilo Montoya, Alejandro Garcés-Ruiz, and Walter Gil-González. Three-Phase Power Flow Tool for Electric Distribution Grids: A Julia Implementation for Electrical Engineering Students. *Ingeniería*, 28(3):e21419, October 2023.
17. Poornachandratejasvi Laxman Bhattar, Naran M. Pindoriya, Anurag Sharma, and R.T. Naayagi. AC-DC multi-phase power flow algorithms for active distribution system analysis. *Electric Power Systems Research*, 226:109924, January 2024.
18. Samuel N Okhuegbe, Adedasola A Ademola, and Yilu Liu. A Machine Learning Initializer for Newton-Raphson AC Power Flow Convergence. *2024 IEEE Texas Power and Energy Conference (TPEC)*, pages 1–6, March 2024.
19. Yu Chen and ZhangJie Liu. Convergence Analysis of Newton-Raphson Method in Lossless Power-flow for Radial Networks. *2023 2nd Asia Power and Electrical Technology Conference (APET)*, pages 693–698, 2023.
20. Soumen Pal, Manojit Bhattacharya, Snehasish Dash, Sang-Soo Lee, and Chiranjib Chakraborty. A next-generation dynamic programming language julia: Its features and applications in biological science. *Journal of Advanced Research*, 64:143–154, October 2024.
21. Sunil Rawan. MATLAB: A Comprehensive Platform for Scientific Computing and Engineering Applications. *Journal of Emerging Technologies and Innovative Research*, 12(7), 2025.
22. Javier Jiménez-Ruiz, Andrés Honrubia-Escribano, and Emilio Gómez-Lázaro. Combined Use of Python and DIgSILENT PowerFactory to Analyse Power Systems with Large Amounts of Variable Renewable Generation. *Electronics*, 13(11):2134, May

2024.
23. Julia Uruel-Sanz and Oscar Perpiñán-Lamigueiro. Power Flow Analysis in Urban Distribution Networks with Implementation of Grid-Connected Photovoltaic Systems. *Solar*, 2(1):32–51, February 2022.
24. Oscar Danilo Montoya, Juan S. Giraldo, Luis Fernando Grisales-Noreña, Harold R. Chamorro, and Lazaro Alvarado-Barrios. Accurate and Efficient Derivative-Free Three-Phase Power Flow Method for Unbalanced Distribution Networks. *Computation*, 9(6):61, May 2021.
25. Estrella Parra, Hernando Díaz, Andrei Romero, and Aldemar Guerra. Power Systems Analysis with MATLAB (In Spanish). *Ingeniería e Investigación*, (41):10–15, September 1998.
26. Brandon Cortés-Caicedo, Laura Sofía Avellaneda-Gómez, Oscar Danilo Montoya, Lazaro Alvarado-Barrios, and Harold R. Chamorro. Application of the Vortex Search Algorithm to the Phase-Balancing Problem in Distribution Systems. *Energies*, 14(5):1282, February 2021.
27. Alexander Emanuel Torres Romero, David Humberto Cárdenas Villacres, and Raquel de los Angeles Salas Ibarra. Análisis de Flujo AC Aplicados a un Sistema Eléctrico de Potencia. *INGENIO*, 7(1):47–56, ene. 2024.
28. Roberto Gabriel Sumba Cáceres. Herramientas computacionales para la realización de flujos de potencia en sistemas eléctricos. *Trabajo de Integración Curricular*, page 82, apr. 2023.
29. Bohang Fang, Changhong Zhao, and Steven H. Low. On the Convergence of Backward/Forward Sweep for Power Flow Solution in Radial Networks. *IEEE Transactions on Control of Network Systems*, 12(2):1780–1792, 2025.
30. Chang Yang and Zhengshuo Li. Distributed Conditional-Distributionally Robust Coordination for an Electrical Power and Flexibility-Enhanced District Heating System. *Applied Energy*, 347:121491, 2023.
31. Yiting Jin, Zhaoyan Wang, Da Xu, Zhenchong Wu, and Shufeng Dong. Coordinated Optimization of Distribution Networks and Smart Buildings Based on Anderson-Accelerated ADMM. *Electronics*, 15(6):1313, 2026.
32. Jiandong Wo, Xiao Qian, Shufeng Dong, Yiwen Xie, Leiyan Lv, and Xuan Fang. Distributed Optimal Scheduling of Multiple Integrated Energy Systems Based on Anderson Accelerated ADMM. In *2024 China International Conference on Electricity Distribution (CICED)*, pages 246–254. IEEE, 2024.
33. Frederik Geth, Sander Claeys, and Rahmat Heidari. On the Implementation of the Fixed Point Iteration Current Injection Method to Solve Four-Wire Unbalanced Power Flow in PowerModelsDistribution.jl. *arXiv preprint*, May 2023.
34. Xinrui Wang, Wengang Chen, Ruimin Tian, Yuze Ji, and Jianfei Zhu. Fast Power Flow Calculation for Distribution Networks Based on Graph Models and Hierarchical Forward-Backward Sweep Parallel Algorithm. *Frontiers in Energy Research*, 12:1465900, 2024.
35. Namami Krishna Sharma, Rohit Kumar, S. C. Choube, and Rajesh Arya. Linear Regression-Based Machine Learning Model for Dynamic Load Flow Analysis. In *2023 IEEE Renewable Energy and Sustainable E-Mobility Conference (RESEM)*, pages 1–6. IEEE, 2023.
36. Deepak Tiwari, Mehdi Jabbari Zideh, Veeru Talreja, Vishal Verma, Sarika Khushalani Solanki, and Jignesh Solanki. Power Flow Analysis Using Deep Neural Networks in Three-Phase Unbalanced Smart Distribution Grids. *IEEE Access*, 12:29959–29970, 2024.
37. Mauricio Alexander Jiménez Cuaces. Flujo óptimo de Potencia: Desarrollo de Procesador de Topología usando Python y DIgSILENT, September 2023.
38. Álvaro Marrón Borrego. Procedimiento alternativo para la inclusión de límites de potencia reactiva en el flujo de cargas. Trabajo fin de máster, Universidad de Sevilla, Sevilla, España, 2025. Departamento de Ingeniería Eléctrica, Escuela Técnica Superior de Ingeniería.
39. L. F. Grisales-Noreña, J. C. Morales-Duran, S. Velez-Garcia, Oscar Danilo Montoya, and Walter Gil-González. Power flow methods used in ac distribution networks: An analysis of convergence and processing times in radial and meshed grid configurations. *Results in Engineering*, 17:100915, 2023.
40. Edgar Mauricio Salazar Duque, Juan S. Giraldo, Pedro P. Vergara, Phuong H. Nguyen, and Han (J.G.) Slootweg. Tensor power flow formulations for multidimensional analyses in distribution systems. *International Journal of Electrical Power & Energy Systems*, 162:110275, 2024.